Steel and Composite Structures, *Vol. 31, No. 6 (2019) 601-615*
DOI: https://doi.org/10.12989/scs.2019.31.6.601

Experimental and numerical investigations on axial strength of back-to-back built-up cold-formed steel angle columns

G. Beulah Gnana Ananthi [1a], Krishanu Roy [*2] and James B.P. Lim [2b]

[1] *Division of Structural Engineering, College of Engineering Guindy Campus, Anna University, Chennai, India*
[2] *Department of Civil and Environmental Engineering, The University of Auckland, Auckland, New Zealand*

(*Received January 25, 2019, Revised April 17, 2019, Accepted May 3, 2019*)

Abstract. In cold-formed steel (CFS) structures, such as trusses, wall frames and columns, the use of back-to-back built-up CFS angle sections are becoming increasingly popular. In such an arrangement, intermediate fasteners are required at discrete points along the length, preventing the angle-sections from buckling independently. Limited research is available in the literature on the axial strength of back-to-back built-up CFS angle sections. The issue is addressed herein. This paper presents the results of 16 experimental tests, conducted on back-to-back built-up CFS screw fastened angle sections under axial compression. A nonlinear finite element model is then described, which includes material non-linearity, geometric imperfections and explicit modelling of the intermediate fasteners. The finite element model was validated against the experimental test results. The validated finite element model was then used for the purpose of a parametric study comprising 66 models. The effect of fastener spacing on axial strength was investigated. Four different cross-sections and two different thicknesses were analyzed in the parametric study, varying the slenderness ratio of the built-up columns from 20 to 120. Axial strengths obtained from the experimental tests and finite element analysis were used to assess the performance of the current design guidelines as per the Direct Strength Method (DSM); obtained comparison showed that the DSM is over-conservative by 13% on average. This paper has therefore proposed improved design rules for the DSM and verified their accuracy against the finite element and test results of back-to-back built-up CFS angle sections under axial compression.

Keywords: back-to-back sections; built-up columns; cold-formed steel; direct strength method; finite element analysis

1. Introduction

Back-to-back built-up cold-formed steel (CFS) angle sections are increasingly used as compression members in structures. Applications include struts in steel trusses and space frames, wall studs in wall frames, and columns and rafters. In such an arrangement, intermediate fasteners at discrete points along the length are used to prevent the channel sections from buckling independently. The American Iron and Steel Institute (AISI 2016) and Australian and New Zealand standards (AS/NZS 2018), both prescribe the same modified slenderness approach to consider the spacing of fasteners in built-up columns. It should be noted that the modified slenderness approach has been adapted from the design guidance of hot-rolled steel structures.

In the literature, very limited research has been described for back-to-back screw fastened built-up CFS angle sections under axial compression, in the arrangement shown in Fig. 1. However, research is available on the back-to-back built-up CFS welded angle sections under axial compression (Vishnuvardhan 2006). For CFS built-up box sections, formed by connecting two angle sections, Beulah (2018) conducted experimental and numerical investigations.

CFS single angle section columns were studied extensively by previous researchers. Young and Chen (2008) conducted column tests on CFS non-symmetric lipped angle sections. Shi *et al*. (2011) conducted experimental tests and finite element analysis on the local buckling of 420 MPa steel equal angle columns under axial compression. Ellobody and Young (2007) studied the design of CFS unequal angle compression members. However, it should be mentioned that all these investigations were different from the built-up section investigated in this paper. No research has been done to investigate the axial strength of back-to-back screw-fastened built-up CFS angle sections.

In terms of CFS built-up columns formed by connecting two back-to-back channels, significant research is available in the literature. Dabaon *et al*. (2015) considered built-up sections, which were steel battened columns connecting two back-to-back channels using batten plates, it was found that both the AISI and the Eurocodes (EN 1993-1-3, 1993) were un-conservative when the steel battened columns failed through local buckling but were conservative when they failed through flexural buckling. While Stone and LaBoube (2005) investigated the axial strength of back-to-back CFS channel sections, these had stiffened flanges and track sections. Whittle and Ramseyer (2009) studied the axial strength of built-up CFS channel sections, which were

*Corresponding author, Ph.D. Student,
E-mail: kroy405@aucklanduni.ac.nz
[a] Associate Professor, E-mail: beulahceg@gmail.com
[b] Associate Professor, E-mail: james.lim@auckland.ac.nz

ISSN: 1229-9367 (Print), 1598-6233 (Online)

welded toe to toe. Welded channels, connected back-to-back, were also investigated by Piyawat *et al*. (2013). Zhang and Young (2012) considered back-to-back built-up CFS channel sections, but with an opening. Ting *et al*. (2018) investigated the effect of screw spacing on the axial strength of CFS built-up back-to-back channels. Roy *et al*. (2018a) extended the work of Ting *et al*. (2018) by investigating the effect of thickness on the axial strength of CFS built-up sections, by connecting two channels back-to-back, with the help of intermediate fasteners. Roy *et al*. (2018b, c) also investigated the axial strength of back-to-back gapped built-up CFS channel sections and proposed design recommendations for such gapped built-up columns. More recently, Roy *et al*. (2018d) studied the axial strength of face-to-face built-up CFS channel sections and showed that AISI & AS/NZS is generally conservative for built-up columns failed through global buckling; however, the AISI & AS/NZS can be un-conservative for columns that fail by local buckling.

For other configurations of CFS built-up sections, extensive research was conducted by previous researchers. Georgieva *et al*. (2012) considered built-up columns composed of zed-sections which were connected toe-to-toe. A new approach for the design of double-Z CFS members based on the direct strength method was proposed by Georgieva *et al*. (2012). Other works include that of Fratamico *et al*. (2018) and Anbarasu *et al*. (2015) who investigated the global buckling strength of built-up CFS built-up channels and CFS web stiffened built-up batten columns, respectively. On the other hand, Liao *et al*. (2017) investigated multi-limbs built-up CFS stub columns under compression and concluded that the fastener spacing has a little impact on the ultimate axial strength of the multi-limbs built-up CFS stub columns. Biggs *et al*. (2015) investigated the axial strength of rectangular and I-shaped welded built-up CFS columns under compression and concluded that AISI (2016) can be more conservative for thicker members but less conservative for wider members. Recently, Yan *et al*. (2017) conducted an experimental investigation and developed a novel direct strength method for design of CFS built-up I section columns. On the other hand, Dar *et al*. (2018) investigated the behaviour of laced built-up CFS columns, through experimental and numerical investigations. Dar *et al*. (2015) also conducted experimental tests on different innovative cross sections of CFS beams with different stiffening arrangements. Recently, Roy *et al*. (2018d), investigated the axial strength of back-to-back built-up CFS un-lipped channels under axial compression and reported that AISI & AS/NZS can be un-conservative by around 8% for columns which failed through local buckling. Furthermore, Kim *et al*. (2015) presented a new shape of the built-up welded square steel tubes, called the ACT tube, to be used as a new scheme of stiffened concrete filled steel tube, which gave higher strength and ductility than regular hot rolled steel sections.

In terms of using modified slenderness approach, Whittle and Ramseyer (2019) recommended using the modified slenderness approach to calculate the axial strength of CFS built-up members. On the other hand, for CFS built-up welded box columns, Reyes and Guzman (2011) found that the modified slenderness ratio could be used in place of the actual slenderness ratio for material thicknesses of 1.5 and 2.0 mm, when calculating the ultimate load capacity of built-up box sections if the seam weld spacing is less than or equal to 600 mm. However, it should be mentioned that all these investigations were different from the built-up section investigated in this paper. No research has been done to investigate the axial strength of back-to-back screw-fastened built-up CFS angle section columns.

This paper presents an experimental investigation on the axial strength of back-to-back built-up CFS screw fastened angle sections. In total, 16 test results are reported. Four different types of cross-sections of back-to-back built-up CFS angle sections with two different thicknesses were considered in the experimental investigation. The material properties were determined using the tensile coupon tests. The effect of slenderness, fastener spacing, load-axial shortening, load-lateral displacement and failure modes of the back-to-back built-up CFS angle sections were investigated in this paper. A non-linear finite element model was then developed, which includes material non-linearity, geometric imperfections and modeling of intermediate fasteners. The FE model was validated against the experimental test results. Using the validated FE model, an extensive parametric study was conducted, comprising 66 models, varying the modified slenderness ratios of the built-up columns from 20 to 120. Axial strengths obtained from the experiments and FEA were used to assess the performance of the current design guidelines as per the Direct Strength Method (DSM). It was found that the current DSM is over-conservative by approximately 13%, while predicting the axial strength of such columns. This paper has therefore proposed an improved design rule for the DSM and verified their accuracy against the tests and FEA results on back-to-back built-up CFS screw fastened angle sections under axial compression.

2. Design guidelines in accordance with the AISI and AS/NZ standards

The un-factored design strengths of back-to-back built-up CFS angle sections can be calculated in accordance with the American Iron and Steel Institute's specification (AISI 2016) and the Australia/New Zealand standards (AS/NZS 2018). The AISI & AS/NZS recommends the use of both the Effective Width Method (EWM) and the Direct Strength Method (DSM) to calculate the buckling strength and the design capacity. The DSM was used in this study. For back to-back built-up CFS angle sections, the un-factored design strength of axially loaded compression members as per the AISI & AS/NZ standards are as follows

$$P_{AISI\&AS/NZS} = A_e F_n \tag{1}$$

The critical buckling stress (F_n) can be calculated as follows

$$\text{For } \lambda_c \le 1.5, \qquad F_n = \left(0.658^{\lambda_c^2}\right) F_y \tag{2}$$

$$\text{For } \lambda_c > 1.5, \qquad F_n = \left(\frac{0.877}{\lambda^2{}_c}\right) F_y \tag{3}$$

The non-dimensional critical slenderness (λ_c) can be calculated as follows

$$\lambda_c = \sqrt{\frac{F_y}{F_e}} \tag{4}$$

According to the AISI and AS/NZS, the modified slenderness ratio can be calculated as per the equation below

$$\left(\frac{KL}{r}\right)_{ms} = \sqrt{\left(\frac{KL}{r}\right)_o^2 + \left(\frac{s}{r_{yc}}\right)^2} \text{ ; For which } \left(\frac{s}{r_{yc}}\right) \le 0.5\left(\frac{KL}{r}\right)_o \tag{5}$$

In terms of using the Direct Strength Method (DSM), the axial strength or un-factored design strength (P_{D1}) is given by the minimal nominal axial strengths for flexural buckling (P_{nle}), local buckling (P_{nl}), and distortional buckling (P_{nd}), as shown in Eq. (6).

$$P_{D1} = \min\left(P_{ne}, P_{nle}, P_{nd}\right) \tag{6}$$

The nominal axial strength (P_{ne}) for flexural buckling is shown in Eq. (7).

$$P_{ne} = \begin{cases} (0.658^{\lambda_c^2})P_y & \lambda_c \le 1.5 \\ \left[\left(\dfrac{0.877}{\lambda_c^2}\right)\right]P_y & \lambda_c > 1.5 \end{cases} \tag{7}$$

$$P_{nle} = \begin{cases} P_{ne} & \lambda_1 \le 0.776 \\ \left[1 - 0.15\left(\dfrac{P_{crl}}{P_{ne}}\right)^{0.4}\right]\left(\dfrac{P_{crl}}{P_{ne}}\right)^{0.4} P_{ne} & \lambda_1 > 0.776 \end{cases} \tag{8}$$

$$P_{nle} = \begin{cases} P_y & \lambda_d \le 0.561 \\ \left[1 - 0.25\left(\dfrac{P_{crd}}{P_y}\right)^{0.6}\right]\left(\dfrac{P_{crd}}{P_y}\right)^{0.6} P_y & \lambda_d > 0.561 \end{cases} \tag{9}$$

Where

$$\lambda_c = \sqrt{\frac{P_y}{P_{cre}}}, \quad \lambda_1 = \sqrt{\frac{P_{ne}}{P_{crl}}}, \quad \lambda_d = \sqrt{\frac{P_y}{P_{crd}}}, \qquad P_y = A_g f_y, \quad P_{crl} = A_g f_{crl}, \quad P_{crd} = A_g f_{crd} \tag{9}$$

In the above equations, A_g is the gross cross-sectional area, P_{cre}, P_{crl} and P_{crd} are the elastic critical local, distortional and overall buckling load, respectively. P_{ne}, P_{nle} and P_{nd} are the nominal overall buckling strength, local-global interaction buckling strength and distortional buckling strength.

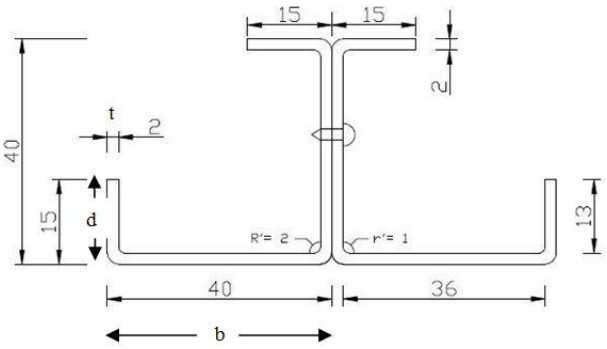

Fig. 1 Details of the back-to-back built-up CFS angle sections (BUA40-t2)

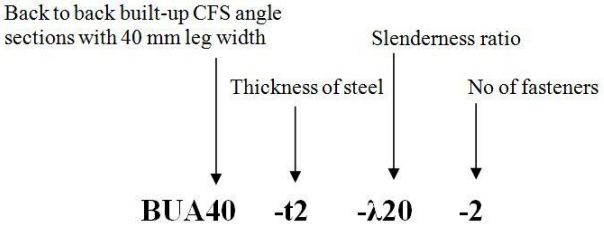

Fig. 2 Specimen labelling

3. Experimental investigation

3.1 Test sections

Fig. 1 shows the details of a typical cross-section (BUA40) considered in the experimental investigation. In total, four different cross sections were considered for the back-to-back built-up CFS angle sections. As indicated by the names, BUA40, BUA50, BUA60 and BUA70 are back-to-back built-up CFS angle sections with 40 mm, 50 mm, 60 mm and 70 mm leg widths, respectively. Two different base-metal thicknesses were considered (2 mm and 3.15 mm) in the experimental investigation. In total, sixteen back-to-back built-up CFS angle sections were tested, subdivided into four different cross sections, two different thicknesses and two different slenderness ratios (Table 1).

Pin-ended boundary conditions were applied in the experiments for all back-to-back built-up CFS angle sections. As shown in Table 1, the test specimens have been sub-divided into stub and short columns. In the experimental test program, all the built-up columns had three intermediate fasteners, irrespective of the column height. The spacing of the fasteners was designed to cover the spacing requirement of the CFS built-up columns as per the clause C4.5 of the AISI (2016) specification.

3.2 Section labels

The built-up sections were labelled such that the type of section, thickness of steel, slenderness ratio, and the number of fasteners, were indicated by the label. Fig. 2 shows an example of the labelling used in the experimental program. As shown in the label, BUA40-t2-λ20-2 is explained as follows:

Table 1 Comparison of test results against FEA and AISI results for back-to-back built-up CFS angle sections

(a) 2 mm thickness

Specimen	Leg	Lip	Length	Spacing	Experimental results	AISI results		FEA results	
	b	d	L	S	P_{EXP}	P_{AISI}	P_{EXP}/P_{AISI}	P_{FEA}	P_{EXP}/P_{FEA}
	(mm)	(mm)	(mm)	(mm)	(kN)	(kN)	-	(kN)	-
BUA40-t2-λ20-3	40	15	286.8	135	108.9	107.0	1.02	115.8	0.94
BUA40-t2-λ30-3	40	15	430.2	205	98.2	100.6	0.98	105.1	0.94
BUA50-t2-λ20-3	50	15	356.8	165	134.6	124.1	1.08	136.2	0.99
BUA50-t2-λ30-3	50	15	535.2	255	112.6	112.6	1.00	120.0	0.94
BUA60-t2-λ20-3	60	15	425.6	200	137.3	138.6	0.99	153.9	0.89
BUA60-t2-λ30-3	60	15	638.4	305	118.9	120.1	0.99	129.4	0.92
BUA70-t2-λ20-3	70	15	493.5	235	140.3	149.9	0.94	169.0	0.83
BUA70-t2-λ30-3	70	15	740.3	360	120.4	122.8	0.98	138.8	0.87
Mean	-	-	-	-	-	-	1.00	-	0.91
COV	-	-	-	-	-	-	0.04	-	0.05

(b) 3.15 mm thickness

Specimen	Leg	Lip	Length	Spacing	Experimental results	AISI results		FEA results	
	b	d	L	S	P_{EXP}	P_{AISI}	P_{EXP}/P_{AISI}	P_{FEA}	P_{EXP}/P_{FEA}
	(mm)	(mm)	(mm)	(mm)	(kN)	(kN)	-	(kN)	-
BUA40-t3.15-λ20-3	40	15	275.7	125	238.3	230.4	1.03	236.1	1.01
BUA40-t3.15-λ30-3	40	15	413.6	195	227.6	214.1	1.06	230.1	0.99
BUA50-t3.15-λ20-3	50	15	345.5	160	274.7	266.2	1.03	280.5	0.98
BUA50-t3.15-λ30-3	50	15	518.2	245	262.8	237.8	1.11	266.0	0.99
BUA60-t3.15-λ20-3	60	15	401.4	190	307.9	297.3	1.04	313.9	0.98
BUA60-t3.15-λ30-3	60	15	602.1	290	276.9	254.4	1.09	292.2	0.95
BUA70-t3.15-λ20-3	70	15	481.6	230	325.7	325.6	1.00	343.9	0.95
BUA70-t3.15-λ30-3	70	15	722.4	350	295.1	265.6	1.11	300.8	0.98
Mean	-	-	-	-	-	-	1.06	-	0.98
COV	-	-	-	-	-	-	0.04	-	0.02

- "BUA40" indicates back-to-back built-up CFS angle sections with 40 mm leg width.
- "t2" indicates the thickness of steel as 2 mm.
- "λ20" indicates the slenderness ratio of 20.
- "2" indicates the numbers of fasteners used as 2.

3.3 Material testing

Tensile coupon tests were conducted to determine the material properties of the test specimens. The tensile coupons were cut from the center of the back-to-back angle sections in accordance with the ASTM A 370 (1996). Three coupons were obtained from the longitudinal directions of the back-to-back angle sections for both the thicknesses (2 mm and 3.15 mm). The coupons were tested in an UTM (Universal testing machine) which has a capacity of 500 kN. A calibrated extensometer of 50 mm gauge length was used to determine the tensile strain of the coupons. From the results of the tensile coupon tests, the average values of the Young's modulus and yield strength were 200 GPa and 282.67 MPa, respectively for 2 mm thick angle sections. Whereas for 3.15 mm thick angle sections, the Young's modulus and yield strength were 210 GPa and 419.23 MPa, respectively.

3.4 Testing-rig and loading procedure

Back-to-back built-up CFS angle sections were tested under pin ended boundary conditions. Two square end plates (200 mm × 200 mm) of 6 mm thickness were welded to the ends of the specimens. The axial load was applied through the center of gravity (CG) of the built-up columns. To simulate the pin ended boundaries, two base plates (120 mm × 120 mm) of 12 mm thickness were used (Fig. 3). A photograph of the test set-up is shown in Fig. 4. The external load cell was placed at the bottom of the built-up column. Three dial gauges were used for each test. Dial gauge positions are numbered as 1, 2 and 3 in Fig. 4. Dial gauge-1 was used to determine the axial shortening of the built-up column. Dial gauge-2 and 3 were used to determine the lateral displacements at the mid-height and one third height of the columns from the bottom base plate, respectively. A Universal Testing Machine (UTM), of 500 kN capacity, was used to apply the axial load to the

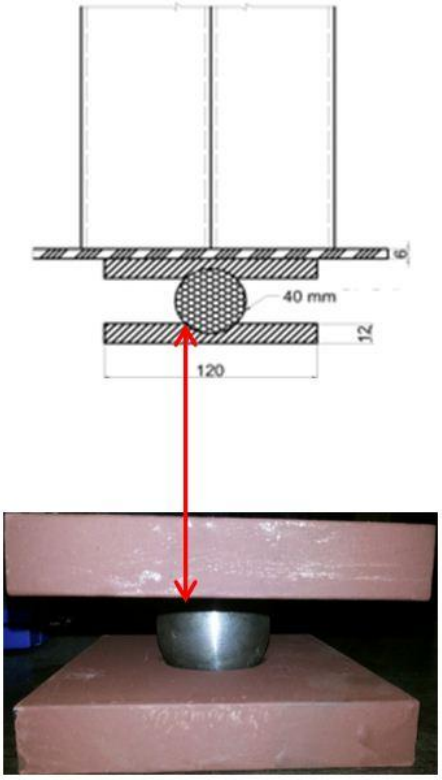

Fig. 3 Details of experimental test set up

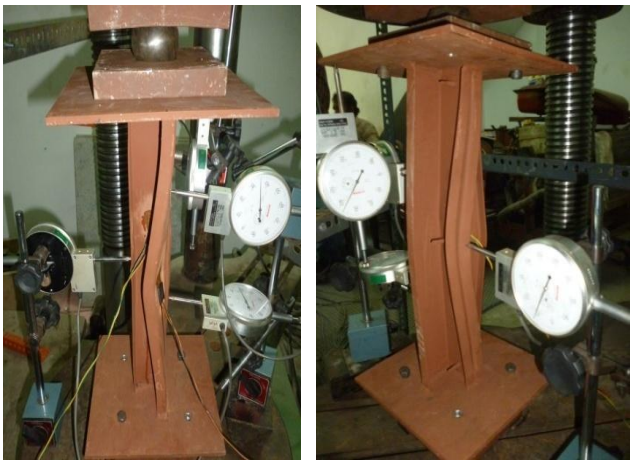

(a) BUA60-t2-λ30-3

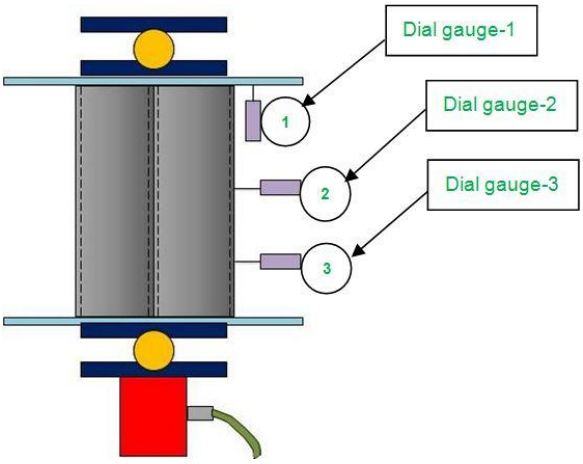

(b) BUA70-t2-λ30-3

Fig. 4 Photograph of experimental test set-up

back-to-back built-up CFS angle sections. The displacement control method was used to apply the axial load. The benefit of using the displacement control is that, it can predict the post-buckling behaviour of the built-up columns. Displacement rate was kept as 0.01 mm/s for all test specimens. All sensors including the dial gauge and load cell readings were recorded with each increment of loading.

3.5 Experimental results

The dimensions of the test specimens along with their experimental (P_{EXP}), and design strengths in accordance with the AISI & AS/NZS (P_{AISI}) are shown in Tables 1(a) and 1(b) for 2 mm and 3.15 mm thick built-up columns, respectively. As can be seen from Tables 1(a) and 1(b), the axial strength of back-to-back built-up CFS angle sections significantly reduced with increase in slenderness ratio. In the experimental tests, all columns having slenderness ratio in the range of 20 to 30, failed through a combination of local and flexural-torsional buckling.

Load-axial shortening relationship for BUA60-t3.15-λ20-3 is plotted in Fig. 5. It is shown that the relationship is almost linear up to a load of 225kN, which is 73% of the ultimate failure load for BUA60-t3.15-λ20-3. After that, the non-linear behavior is continued until the failure load is reached, which is 307.90 kN. The back-to-back built-up CFS angle sections, having leg widths of 40 mm and 50 mm, failed through a combination of local and flexural-torsional buckling, irrespective of their slenderness ratios. Whereas the back-to-back built-up CFS angle sections,

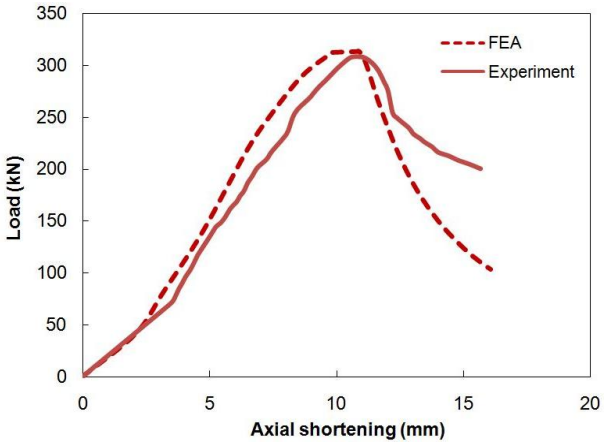

Fig. 5 Load verses axial displacement curves from experimental tests and FE results for BUA60-t3.15-λ20-3

having 60 mm and 70 mm leg widths, failed by a combination of local and flexural buckling. Figs. 6 and 7 show the load versus lateral deflection behaviour for BUA40-t2-λ20-3 and BUA70-t3.15-λ30-3, respectively. For BUA40-t2-λ20-3, the lateral displacements increased

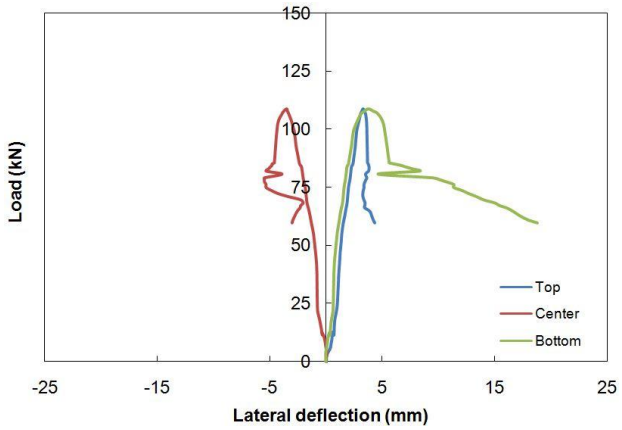

Fig. 6 Load versus lateral displacement curves from the tests and FE results forBUA40-t2-λ20-3

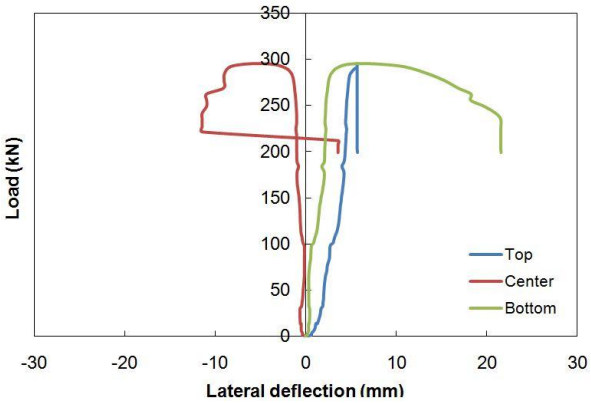

Fig. 7 Load versus lateral displacement curves from the tests and FE results for BUA70-t3.15-λ20-3

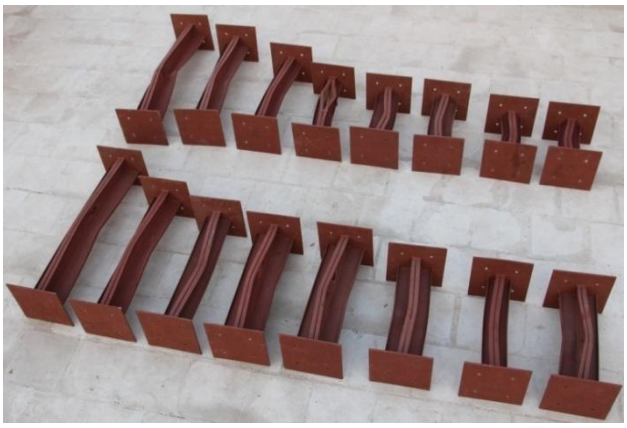

Fig. 8 Photograph of the back-to-back built-up CFS angle sections at failure from experiments

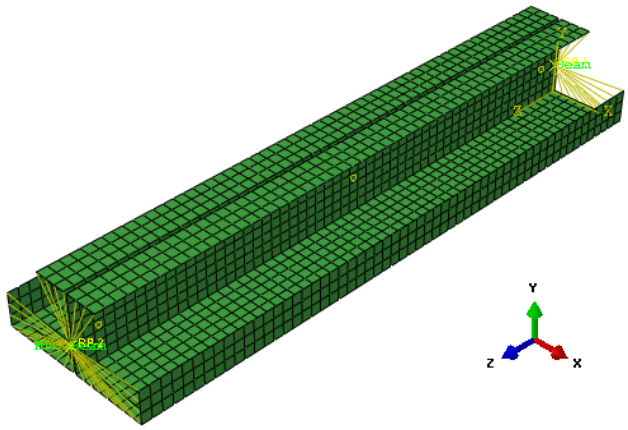

Fig. 9 Typical finite element mesh for BUA40-t2-λ20-3

slowly, showing large inward deflection, with increasing load. On the other hand, large outward deflection was noticed in the bottom of the column for BUA40-t2-λ20-3. No significant increase in the deflection was observed for a load up to 10% of the failure load for BUA70-t3.15-λ30-3. Fig. 8 shows the failure modes of back-to-back built-up CFS angle sections from the experiments.

4. Numerical investigation

4.1 General

ABAQUS (2018) was used to develop a non-linear elasto-plastic finite element model for back-to-back built-up CFS angle sections under axial compression. The finite element model was based on the centerline dimensions of the cross-section of built-up angle sections. Two types of finite element analysis were performed. The buckling modes of the built-up columns were determined, first, through the eigenvalue analysis, which is a linear elastic analysis performed using the (*BUCKLE) procedure available in the ABAQUS library. A load-displacement nonlinear analysis was then carried out using RIKS algorithm available in the ABAQUS library. The geometric imperfections and material nonlinearities were included in the finite element model. Specific modeling issues are described in the following sections.

4.2 Geometry and material properties

The full geometry of the back-to-back built-up CFS angle sections was modelled. True values of stresses and strains were specified in the finite element model to incorporate the material non-linearities. The ABAQUS classical metal plasticity model was used for the analysis and validation purpose. Isotropic yielding, associated plastic flow theory, and isotropic hardening behavior was considered. For the parametric study, a simplified elastic perfect plastic stress–strain curve obeying Von Mises yield criterion was used. Yield stress, ultimate stress, along with Young's modulus values were considered from the results of the coupon tests described in the experimental section (section 3.2). From the coupon test results, the average values of the Young's modulus and yield strength were 200 GPa and 282.67 MPa, respectively for 2 mm thick angle sections. Whereas for 3.15 mm thick angle sections, the Young's modulus and yield strength were 210 GPa and 419.23 MPa, respectively. These values were considered in the FE models developed in this study. As per the ABAQUS manual, the engineering

material curve was converted into a true material curve in the FE analysis by using the following equations

$$\sigma_{true} = \sigma(1+\varepsilon) \tag{10}$$

$$\varepsilon_{true(pl)} = \ln(1+\varepsilon) - \frac{\sigma_{true}}{E} \tag{11}$$

Where E is the Young's Modulus, σ and ε is the engineering stress and strain respectively in ABAQUS (2018).

4.3 Element type and finite element mesh

A linear 4-noded quadrilateral thick shell element (S4R5), available in ABAQUS element library, was used to model the built-up sections. A mesh size of 5 mm × 5 mm (length×width) was used for the convergence of the model.

Along the length of the sections, the number of elements was chosen so that the aspect ratio of the elements was close to one. A mesh sensitivity analysis was performed to verify the number of elements. A typical finite element mesh is shown in Fig. 9 for BUA40-t2-λ20-3.

4.4 Boundary conditions and load application

Pin-ended boundary conditions were applied for all built-up columns. In order to simulate pin-ended boundary conditions, displacements and rotations were applied to the upper and lower ends of the back-to-back built-up CFS angle sections through the reference points. The reference point was considered as the center of gravity (CG) of the cross section of the back-to-back built-up CFS angle sections. Fasteners between the back-to-back angles were modelled using the MPC beam connector elements available in the ABAQUS library (Fig. 10(a)). The load was applied to the reference points of the built-up angle sections as shown in Fig. 10(b). The RIKS algorithm, available in the ABAQUS library, was used to apply the load in increments. By using the RIKS method, post buckling behaviour of the back-to-back built-up CFS columns can be predicted (Roy *et al*. 2018c).

4.5 Contact modelling

"*Surface to surface*" contact was used for modeling the interaction between the webs of back-to-back angle sections. The web of one angle section was modeled as slave surface, while the web of other angle section was considered as master surface. There was no penetration between the two contact surfaces.

4.6 Modelling of initial imperfections

Local, distortional and overall buckling behavior of the back-to-back built-up CFS angle sections depends on many factors such as: Depth of angle-thickness ratio (D/t), width

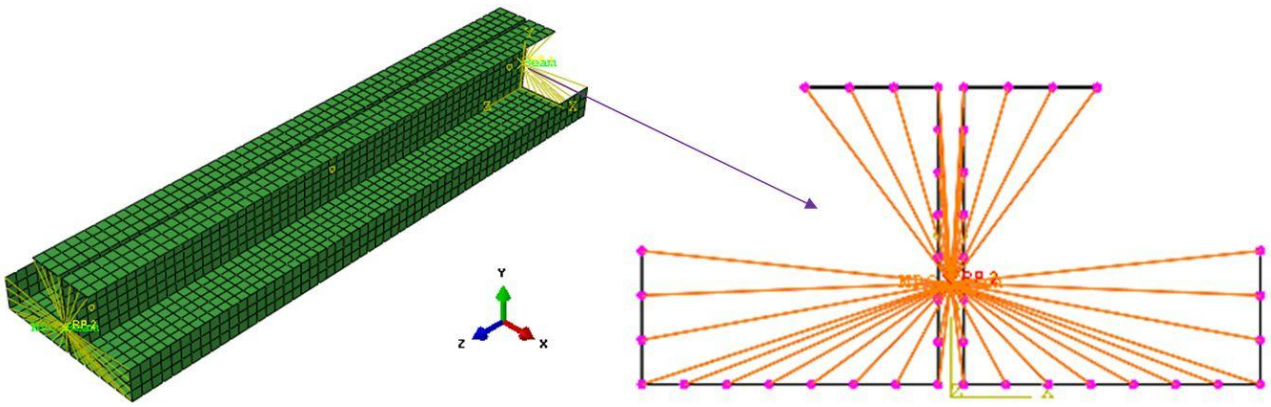

(a) Boundary conditions applied using multi Point Constraints (MPCs)

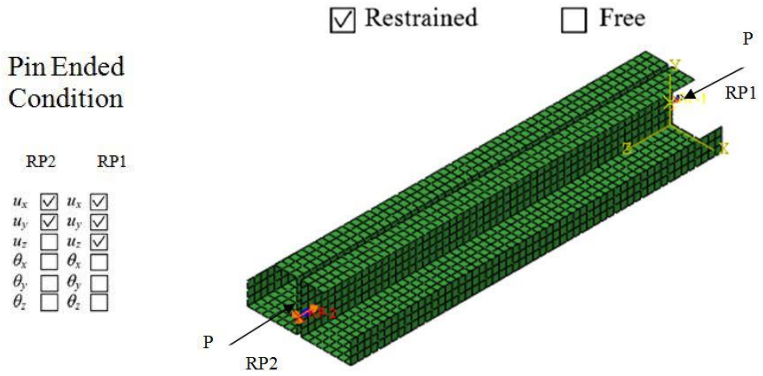

(b) Load application

Fig. 10 Boundary condition and load application in the FE model (BUA40-t2- λ20-3)

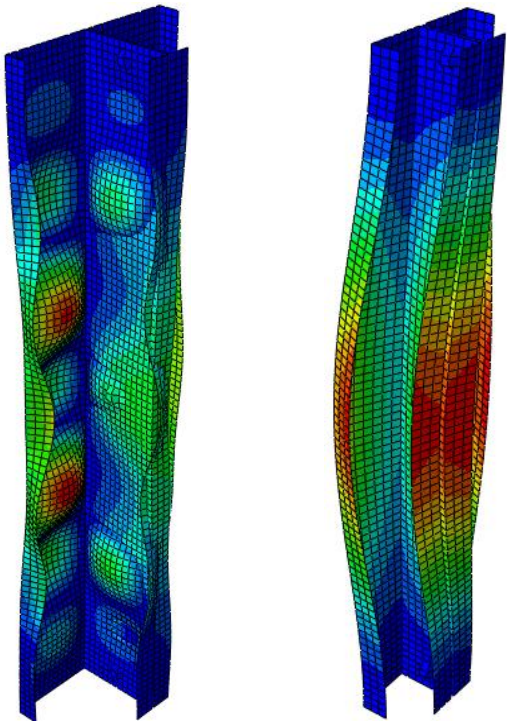

(a) Local buckling (BUA70-t2-λ20-3) (b) Distortional buckling (BUA50-t3.15-λ30-3)

Fig. 11 Initial imperfection contours

of angle-thickness ratio (b/t), slenderness around *x* and *y* axis and spacing of intermediate fasteners. The initial imperfections are caused in compression members as a result of the fabrication process. Distortional buckling is one of the important modes of buckling (Zhou and Jiang (2017)), which was considered in the FE modelling. Local, distortional and overall buckling modes were superimposed for accurate finite element analysis. Eigenvalue analyses of the built-up columns were performed with very small to large angle thickness to determine the contours for the local, distortional and overall imperfections. The lowest buckling mode (Eigen mode 1) in ABAQUS (2018), was used as the shape of local and overall buckling modes. The magnitude of the local, distortional and overall imperfections was considered as 0.006*w*t, 1.0*t and 1/1000 of the full length of the column, respectively, following the recommendations of Schafer and Pekoz (1998). The local and distortional buckling modes of BULA70-S1-λ20-3 and BULA50-S1-λ30-3, obtained from the FEA, are shown in Fig. 11.

4.7 Modelling of residual stresses

Residual stresses can be incorporated into the FE model as initial state using the ABAQUS (*INITIAL CONDITIONS, TYPE = STRESS) option. However, previous studies detailed in Roy *et al*. (2018c), Schafer and Pekoz (1998) showed that it has a negligible effect on the column strength, stiffness of the built-up column, load-axial shortening behaviour and failure modes. Therefore, residual stresses were not included in the FE model to avoid the complexity of the analysis.

4.8 Finite element model validation

In order to validate the FE model, the test results presented in section 3 are compared against the FEA results (Table 1). Fig. 12 shows the failure modes of BUA40-t2-λ20-3, BUA50-t3.15-λ30-3 and BUA50-t3.15-λ20-3 columns obtained from the experimental tests and FEA for back-to-back built-up CFS angle sections. As can be seen, the experimental and FEA results show good agreement for both ultimate strength and failure modes.

(i) Experimental (ii) FEA (i) Experimental (ii) FEA (i) Experimental (ii) FEA

(a) BUA40-t2- λ20-3 (b) BUA50-t3.15- λ30-3 (c) BUA50-t3.15- λ20-3

Fig. 12 Back-to-back built-up CFS angle sections at failure

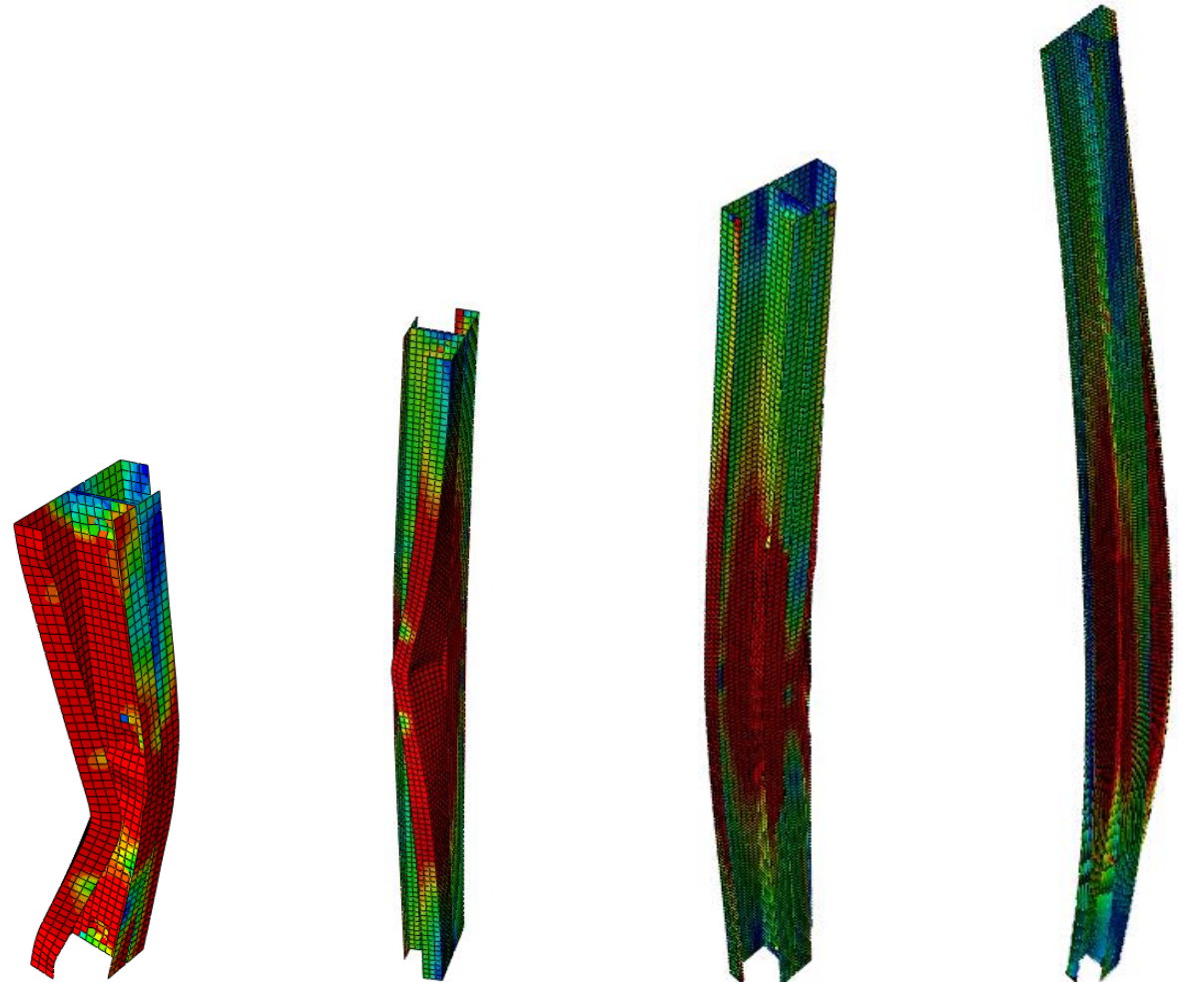

(a) Stub (BUA40-t2-λ20-3) (b) Short (BUA40-t2-λ40-3) (c) Intermediate (BUA40-t2-λ60-4) (d) Slender (BUA40-t2-λ120-6)

Fig. 13 FEA failure modes of back-to-back built-up CFS angle sections

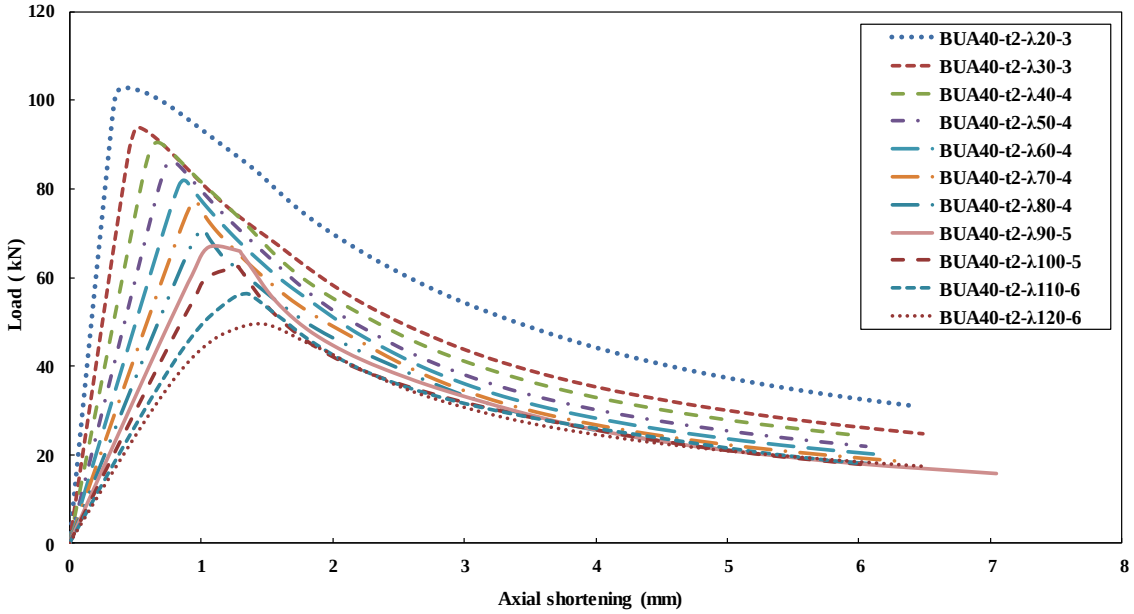

Fig. 14 Load-axial shortening relationship for BUA40-t2 series

Tables 1(a) and 1(b) compare the failure loads obtained from the experimental tests with that of the FEA strength for 2 mm and 3.15 mm thick built-up sections, respectively. It is shown that the mean values of the ratio P_{EXP}/P_{AISI} is 1.00; with a co-efficient of variation of 0.04 and P_{EXP}/P_{FEA} is 0.91, with a co-efficient of variation of 0.05 for 2 mm thick columns of BUA-t2 series. On the other hand, for 3.15 mm thick built-up sections, the mean value of the ratio P_{EXP}/P_{AISI} is 1.06, with a co-efficient of variation of 0.04 and the mean value of P_{EXP}/P_{FEA} is 0.98, with a co-efficient of variation of 0.02. For all specimens, the FEA strengths (P_{FEA}) were higher than the design strengths predicted by the AISI (P_{AISI}).

5. Parametric study

In order to verify the accuracy of the current design guidelines by the Direct Strength Method (DSM), an extensive parametric study was conducted using the validated FE model. In total, 66 FE models were analyzed. In the parametric study, four different cross-sectional dimensions, different lengths, thicknesses and different fastener's spacing were considered. The experimental and FE strengths were compared against the design strength calculated using the DSM.

As can be seen from Fig. 13, significant strength reduction occurred for all columns having slenderness beyond 80. The failure modes of BUA40-t2-λ20-3, BUA40-t2-λ40-3, BUA40-t2-λ60-4 and BUA40-t2-λ120-6 are shown in Figs. 13(a), 13(b), 13(c) and 13(d), respectively. Load-axial shortening curves are shown in Fig. 14 for BUA40-t2 series, with varying λ from 20 to120 and different number of screws fasteners.

To investigate the effect of fastener spacing on the axial strength of back-to-back built-up CFS angle sections, fastener's spacing was varied from 125 mm to 385 mm. The built-up angle sections having λ from 20 to 40, failed due to a combination of local and flexural-torsional buckling. The intermediate and slender columns failed at the mid-height for most of the built-up columns. Table 2 shows the mean value of P_{FEA}/P_{AISI} as 1.13 with a coefficient of variation of 0.08. As can be seen from Table 2, the current DSM overestimates the design strength by around 13% on average. Fig. 15 shows the relationship between the FEA and DSM results in which the variation is almost linear.

The parametric study was further extended to modify the DSM equations to achieve a good fit between the FEA and DSM results. For this purpose, a regression analysis was conducted. The regression co-efficient was 0.96 and the best regression fit was obtained when the equation 12 was used to compare the data points obtained from the FEA and the design strengths using DSM

$$P_{FEA} = 1.121 \times P_{DSM} \quad (12)$$

Based on the results from FEA, the above modification is proposed to the current DSM. This linear equation was then used to predict the axial strength of the back-to-back built-up CFS angle sections. The proposed design equation (Eq. (12)) predicted the design strength of the CFS back-to-back built-up CFS angle sections, more accurately when compared against the FEA results. Fig. 16 shows the variation of P_{DSM}/P_{FEA} and $P_{proposed}/P_{FEA}$ with a dimensionless slenderness ratio. It also shows the variation of P_{DSM}/P_{FEA} where P_{DSM} is the design strength calculated from the current DSM and $P_{proposed}/P_{FEA}$, where $P_{proposed}$ is the design strength obtained from the proposed DSM.

The failure of back-to-back built-up CFS angle sections occurred due to a combination of local and flexural-torsional buckling about the minor axis of the columns. For all the columns having λ greater than 80, location of the failure was observed at the mid-height. As can be seen from Fig. 16, using the existing design method, the axial strength was over-conservative by around 13% to the FEA and test results. However, when the proposed design method was used, the axial strength was within the range (being only 2% conservative) when compared to both the test and FEA results.

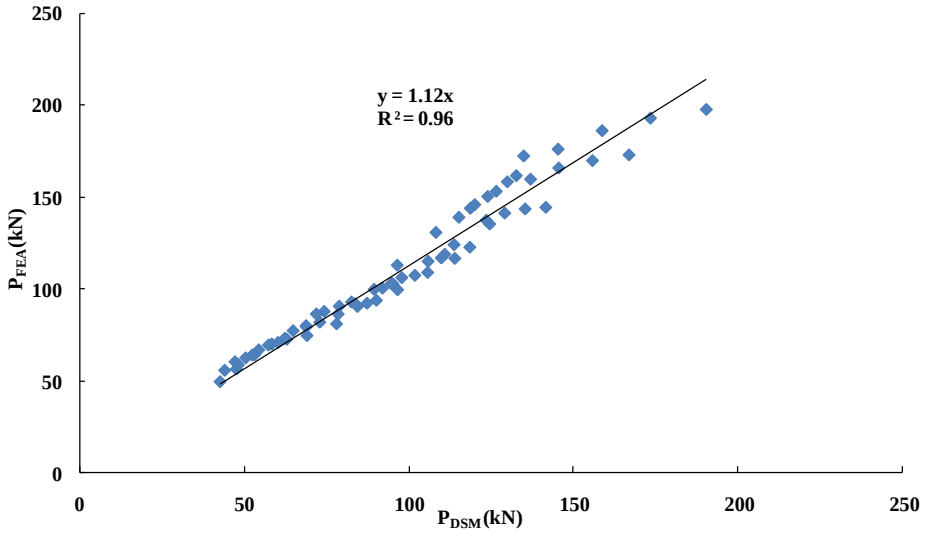

Fig. 15 Comparison of P_{FEA} versus P_{DSM} curve

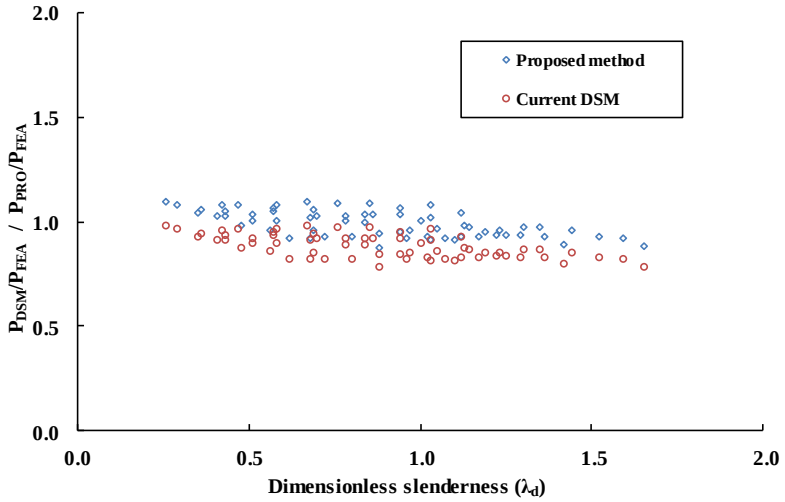

Fig. 16 Comparison of PFEA and PDSM results with dimensionless slenderness ratio

6. Reliability analysis

A reliability analysis was performed according to the procedure given in chapter F of AISI (2016) for assessing the current and modified DSM for the back-to-back built-up CFS angle sections. The capacity reduction factor (φ) was determined from the AISI (2016). The load combination of 1.2DL+1.6LL was used as per the AISI (2016), where DL is the dead load and LL is the live load. The statistical parameters M_m, F_m, V_M and V_F are the mean values and coefficients of variations for material properties and fabrication factors, respectively. These values were taken

Table 2 Finite element strengths and AISI strengths for back-to-back built-up CFS angle sections with varying length and numbers of fasteners

Specimen	Leg b (mm)	Lip d (mm)	Length L (mm)	Spacing S (mm)	P_{FEA} (kN)	P_{DSM} (kN)	$P_{Proposed}$ (kN)	$P_{FEA}/P_{Proposed}$	P_{FEA}/P_{DSM}	Failure modes
BUA40-t2-λ20-3	40	15	286.8	135	102.8	95.4	106.9	0.96	1.08	L+FT
BUA40-t2-λ30-3	40	15	430.2	205	93.8	90.4	101.4	0.93	1.04	L+FT
BUA40-t2-λ40-4	40	15	573.6	185	90.5	84.7	94.9	0.95	1.07	L+F
BUA40-t2-λ50-4	40	15	717.1	230	86.4	78.8	88.4	0.98	1.09	L+F
BUA40-t2-λ60-4	40	15	860.4	280	81.9	73.2	82.1	1.00	1.12	L+F
BUA40-t2-λ70-4	40	15	1003.8	325	77.3	65.2	73.0	1.06	1.13	L+F
BUA40-t2-λ80-4	40	15	1147.2	375	70.8	60.6	67.9	1.04	1.11	L+F
BUA40-t2-λ90-5	40	15	1290.6	315	66.8	54.7	61.4	1.09	1.19	L+F
BUA40-t2-λ100-5	40	15	1434.0	350	62.4	50.7	56.9	1.10	1.20	L+F
BUA40-t2-λ110-6	40	15	1577.4	310	56.4	47.9	53.7	1.05	1.15	L+F
BUA40-t2-λ120-6	40	15	1720.8	340	49.5	42.9	48.2	1.03	1.15	L+F
BUA50-t2-λ20-3	50	15	356.9	165	118.9	111.2	124.6	0.95	1.07	L+F
BUA50-t2-λ30-3	50	15	535.3	255	107.4	102.1	114.5	0.94	1.05	L+FT
BUA50-t2-λ40-4	50	15	713.7	230	100.5	92.3	103.4	0.97	1.09	L+F
BUA50-t2-λ50-4	50	15	892.2	290	92.9	82.9	92.9	1.00	1.12	L+F
BUA50-t2-λ60-5	50	15	1070.6	260	87.8	74.6	83.6	1.05	1.18	L+F
BUA50-t2-λ70-5	50	15	1249.0	305	80.0	69.1	77.4	1.03	1.19	L+F
BUA50-t2-λ80-6	50	15	1427.4	280	72.6	63.2	70.9	1.02	1.20	L+F
BUA50-t2-λ90-6	50	15	1605.9	315	70.0	58.7	65.8	1.06	1.22	L+F
BUA50-t2-λ100-7	50	15	1784.3	290	64.2	53.5	60.00	1.07	1.23	L+F
BUA50-t2-λ110-7	50	15	1962.7	320	58.6	48.5	54.4	1.08	1.25	L+F
BUA50-t2-λ120-8	50	15	2141.2	300	55.7	44.4	49.7	1.12	1.21	L+F

Table 2 Continued

Specimen	Leg b (mm)	Lip d (mm)	Length L (mm)	Spacing S (mm)	P_{FEA} (kN)	P_{DSM} (kN)	$P_{Proposed}$ (kN)	$P_{FEA}/P_{Proposed}$	P_{FEA}/P_{DSM}	Failure modes
BUA60-t2-λ20-3	60	15	425.7	200	135.4	124.8	139.9	0.97	1.09	L+FT
BUA60-t2-λ30-3	60	15	638.5	305	116.9	110.1	123.4	0.95	1.06	L+FT
BUA60-t2-λ40-4	60	15	851.3	275	106.2	98.1	110.0	0.97	1.12	L+F
BUA60-t2-λ50-4	60	15	1064.2	345	99.8	89.7	100.6	0.99	1.14	L+F
BUA60-t2-λ60-5	60	15	1277.0	310	90.6	79.2	88.7	1.02	1.24	L+F
BUA60-t2-λ70-5	60	15	1489.8	365	86.4	72.2	80.9	1.07	1.29	L+F
BUA60-t2-λ80-6	60	15	1702.6	335	79.3	69.2	77.5	1.02	1.33	L+F
BUA60-t2-λ90-6	60	15	1915.5	375	73.1	62.7	70.2	1.04	1.35	L+F
BUA60-t2-λ100-7	60	15	2128.3	350	69.5	57.7	64.7	1.07	1.39	L+F
BUA60-t2-λ110-7	60	15	2341.1	385	64.0	52.8	59.1	1.08	1.36	L+F
BUA60-t2-λ120-8	60	15	2554.0	360	60.3	47.5	53.2	1.13	1.37	L+F
BUA60-t2-λ20-3	60	15	425.7	200	135.4	124.8	139.9	0.97	1.09	L+FT
BUA60-t2-λ30-3	60	15	638.5	305	116.9	110.1	123.4	0.95	1.06	L+FT
BUA60-t2-λ40-4	60	15	851.3	275	106.2	98.1	110.0	0.97	1.12	L+F
BUA60-t2-λ50-4	60	15	1064.2	345	99.8	89.7	100.6	0.99	1.14	L+F
BUA60-t2-λ60-5	60	15	1277.0	310	90.6	79.2	88.7	1.02	1.24	L+F
BUA60-t2-λ70-5	60	15	1489.8	365	86.4	72.2	80.9	1.07	1.29	L+F
BUA60-t2-λ80-6	60	15	1702.6	335	79.3	69.2	77.5	1.02	1.33	L+F
BUA60-t2-λ90-6	60	15	1915.5	375	73.1	62.7	70.2	1.04	1.35	L+F
BUA60-t2-λ100-7	60	15	2128.3	350	69.5	57.7	64.7	1.07	1.39	L+F
BUA60-t2-λ110-7	60	15	2341.1	385	64.0	52.8	59.1	1.08	1.36	L+F
BUA60-t2-λ120-8	60	15	2554.0	360	60.3	47.5	53.2	1.13	1.37	L+F
BUA60-t2-λ20-3	60	15	425.7	200	135.4	124.8	139.9	0.97	1.09	L+FT
BUA40-t3.15-λ20-3	40	15	275.8	125	144.5	141.8	159.0	0.91	1.02	L+FT
BUA40-t3.15-λ30-3	40	15	413.7	195	143.6	135.6	152.0	0.94	1.06	L+FT
BUA40-t3.15-λ40-4	40	15	551.6	175	141.3	129.4	145.0	0.97	1.09	L+F
BUA40-t3.15-λ50-4	40	15	689.5	220	137.5	123.8	138.7	0.99	1.11	L+F
BUA40-t3.15-λ60-5	40	15	827.3	200	122.8	118.8	133.2	0.92	1.03	L+F
BUA40-t3.15-λ70-5	40	15	965.2	235	116.7	114.2	128.0	0.91	1.02	L+F
BUA40-t3.15-λ80-6	40	15	1103.1	215	109.0	106.0	118.8	0.92	1.03	L+F
BUA40-t3.15-λ90-6	40	15	1241.0	240	99.6	96.9	108.6	0.92	1.03	L+F
BUA40-t3.15-λ100-7	40	15	1378.9	225	92.2	87.6	98.2	0.94	1.05	L+F
BUA40-t3.15-λ110-7	40	15	1516.8	250	81.0	78.3	87.8	0.92	1.03	L+F
BUA40-t3.15-λ120-8	40	15	1654.7	230	74.6	69.4	77.7	0.96	1.08	L+F
BUA50-t3.15-λ20-3	50	15	345.5	160	173.1	167.1	187.3	0.92	1.04	L+FT
BUA50-t3.15-λ30-3	50	15	518.3	245	169.9	156.0	174.9	0.97	1.09	L+FT
BUA50-t3.15-λ40-4	50	15	691.0	220	165.9	145.8	163.4	1.02	1.14	L+F
BUA50-t3.15-λ50-4	50	15	863.8	280	159.8	137.2	153.8	1.04	1.16	L+F
BUA50-t3.15-λ60-5	50	15	1036.6	250	158.4	130.2	145.9	1.09	1.22	L+F
BUA50-t3.15-λ70-5	50	15	1209.3	295	150.4	124.2	139.2	1.08	1.21	L+F
BUA50-t3.15-λ80-6	50	15	1382.1	270	144.0	118.9	133.3	1.08	1.21	L+F
BUA50-t3.15-λ90-6	50	15	1554.8	305	124.1	114.0	127.8	0.97	1.09	L+F
BUA50-t3.15-λ100-7	50	15	1727.6	280	115.1	106.1	118.9	0.97	1.08	L+F
BUA50-t3.15-λ110-7	50	15	1900.4	310	103.0	94.9	106.4	0.97	1.08	L+F
BUA50-t3.15-λ120-8	50	15	2073.1	290	91.9	84.0	94.2	0.98	1.09	L+F

Table 2 Continued

Specimen	Leg b (mm)	Lip d (mm)	Length L (mm)	Spacing S (mm)	P_{FEA} (kN)	P_{DSM} (kN)	$P_{Proposed}$ (kN)	$P_{FEA}/P_{Proposed}$	P_{FEA}/P_{DSM}	Failure modes
BUA60-t3.15-λ20-3	60	15	401.4	190	197.8	190.6	213.6	0.93	1.04	L+FT
BUA60-t3.15-λ30-3	60	15	602.1	290	193.1	173.6	194.6	0.99	1.11	L+FT
BUA60-t3.15-λ40-4	60	15	802.8	260	186.3	158.9	178.2	1.05	1.17	L+F
BUA60-t3.15-λ50-4	60	15	1003.6	325	176.2	145.6	163.2	1.08	1.19	L+F
BUA60-t3.15-λ60-5	60	15	1204.3	295	172.5	135.1	151.5	1.14	1.24	L+F
BUA60-t3.15-λ70-5	60	15	1405.0	345	161.8	132.9	149.0	1.09	1.22	L+F
BUA60-t3.15-λ80-6	60	15	1605.7	315	153.2	126.8	142.2	1.08	1.21	L+F
BUA60-t3.15-λ90-6	60	15	1806.4	355	145.9	120.3	134.8	1.08	1.21	L+F
BUA60-t3.15-λ100-7	60	15	2007.1	330	139.1	115.5	129.4	1.07	1.20	L+F
BUA60-t3.15-λ110-7	60	15	2207.8	360	130.8	108.5	121.6	1.08	1.21	L+F
BUA60-t3.15-λ120-8	60	15	2408.5	340	113.0	96.8	108.5	1.04	1.17	L+F
Mean, P_m								1.01	1.13	
COV, V_P								0.07	0.08	
Reliability Index β1 (φ = 0.80)								2.90	3.43	
Reliability Index β2 (φ = 0.85)								2.68	3.19	

* L–Local buckling, F–Flexural buckling, T–Torsional buckling

from Table F_1 of the AISI (2016) for concentrically loaded compression members, where M_m = 1.10, F_m = 1.00, V_m = 0.10 and V_f = 0.05. The statistical parameters P_m and V_p are the mean and coefficient of variation of tested to FEA ratios, respectively (Table 2). A correction factor CP was implemented in the analysis which accounted for the influence due to the number of analysis. AISI (2016) suggests a capacity reduction factor in the range of 0.80 to 0.85 for compression members. AISI (2016) also recommends a reliability index (β) greater than 2.5 for compression members. The reliability index for β-0.8 was 2.90 for $P_{FEA}/P_{proposed,}$ whereas the reliability index for β-0.8 was 3.4 for P_{FEA}/P_{DSM}. On the other hand, for β-0.85 the reliability indices were 2.68 and 3.19 for $P_{FEA}/P_{proposed}$ and P_{FEA}/P_{DSM}, respectively. Therefore, the proposed design equation improved the DSM design rule by keeping the reliability index within the limit (> 2.5) as per the AISI (2016).

7. Conclusions

An experimental test program on the axial strength of back-to-back built-up CFS screw fastened angle sections is presented in this paper. A total of 16 experiments are reported. The material properties were determined using the tensile coupon tests. The failure modes, axial strengths, load-axial shortening and load-lateral displacement relationships are discussed. Effect of the fastener spacing on the axial strength of back-to-back built-up CFS angle sections is also investigated.

A nonlinear finite element model is then presented, which includes non-linear material properties, geometric imperfections and modelling of intermediate fasteners. The Finite element model is validated against the experimental test results, which showed good agreement, both in terms of failure loads and deformed shapes.

The validated FE model is used to perform a parametric study to investigate the effect of fastener spacing, different thicknesses and cross-sectional geometries on the axial strength of back-to-back built-up CFS angle sections. In total, 66 finite element models were analyzed, coving a wide range of slenderness (20 to 120). As expected, the strength of the built-up columns decreased steadily with an increase in slenderness ratio. Irrespective of thickness, all the intermediate and slender columns having modified slenderness ratio in the range of 20 to 30, failed through a combination of local and flexural buckling. The column strengths predicted from the FEA were compared against the axial strengths calculated in accordance with the current design guidelines by the Direct Strength Method (DSM). It was found that the DSM design rules are over-conservative by around 13%, while predicting the design strength of such back-to-back built-up CFS angle section columns.

Using the parametric study results, an improved design equation was proposed over the existing DSM method to predict the axial strength of such back-to-back built-up CFS angle sections. When the proposed DSM equation was used to predict the axial strength of such columns, the design strength was only 2% conservative to the FEA and test results. The reliability of the proposed DSM equation was verified by performing a reliability analysis, which gave the reliability index (β) greater than 2.5. The experimental and numerical results reported in this study along with the proposed DSM equation can be used by the practicing engineers and the researchers for predicting the axial

capacity of back-to-back built-up screw fastened CFS angle sections.

References

ABAQUS (2018), Version 6.14-2, SIMULIA, Providence, RI, USA.

American Iron and Steel Institute (2016), North American specification for the design of cold-formed Steel Structural Members; NAS S100.

Anbarasu, M., Kanagarasu, K. and Sukumar, S. (2015), "Investigation on the behaviour and strength of cold-formed steel web stiffened built-up battened columns", *Mater. Struct.*, **48**(12), 4029-4038.

ASTM: 370-92 (1996), Standard test methods and definitions for mechanical testing of steel products.

Beulah, G.A.G. (2018), "A study on cold-formed steel compound angle section subjected to axial compression", *KSCE J. Civil Eng.*, **22**(5), 1803-1815.

Biggs, K.A., Ramseyer, C., Ree, S. and Kang, T.H.K. (2015), "Experimental testing of cold-formed built-up members in pure compression", *Steel Compos. Struct., Int. J.*, **18**(6), 1331-1351. http://dx.doi.org/10.12989/scs.2015.18.6.1331

BS: 5950 - Part 5 (1987), Structural Use of Steelwork in Building - Code of Practice for Design of Cold-formed Sections British Standards Institution.

Dabaon, M., Ellobody, E. and Ramzy, K. (2015), "Nonlinear behavior of built-up cold-formed steel section battened columns", *J. Constr. Steel Res.*, **110**, 16-28.

Dar, M.A., Yusuf, M., Dar, A.R. and Raju, J. (2015), "Experimental study on innovative sections for cold formed steel beams", *Steel Compos. Struct., Int. J.*, **19**(6), 1599-1610. http://dx.doi.org/10.12989/scs.2015.19.6.1599

Dar, M.A., Sahoo, D.R., Pulikkal, S. and Jain, A.K. (2018a), "Behaviour of laced built-up cold-formed steel columns: Experimental investigation and numerical validation", *Thin-Wall. Struct.*, **132**, 398-409.

EC3 (2006), Eurocode 3: design of steel structures – Part 1-3: General rules – supplementary rules for cold-formed members and sheeting. BS EN 1993-1-3. in: Proceedings of the Brussels: European Committee for Standardization.

Ellobody, E. and Young, B. (2007), "Design of cold-formed steel unequal angle compression members", *J. Constr. Steel Res.*, **45**, 330-338.

Fratamico, D.C., Torabian, S., Zhao, X., Rasmussen, K.J. and Schafer, B.W. (2018), "Experiments on the global buckling and collapse of built-up cold-formed steel columns", *J. Constr. Steel Res.*, **144**, 65-80.

Georgieva, I., Schueremans, L. and Lincy, P. (2012), "Composed columns from cold-formed steel Z-profiles: experiments and code based predictions of the overall compression capacity", *Eng. Struct.*, **37**, 125-134.

Kim, S.H., Yom, K.S. and Choi, S.M. (2015), "A study on the structural performance of new shape built-up square column under concentric axial load", *Steel Compos. Struct., Int. J.*, **18**(6), 1451-1464. http://dx.doi.org/10.12989/scs.2015.18.6.1451

Liao, F., Wu, H., Wang, R. and Zhou, T. (2017), "Compression test and analysis of multi-limbs built-up cold-formed steel stub columns", *J. Constr. Steel Res.*, **128**, 405-415.

Piyawat, K., Ramseyer, C. and Kang, T.H.K. (2013), "Development of an axial load capacity equation for doubly symmetric built-up cold-formed sections", *J. Struct. Eng. Am. Soc. Civil Engr.*, **139**(12), 04013008-04013013.

Reyes, W. and Guzmán, A. (2011), "Evaluation of the slenderness ratio in built-up cold-formed box sections", *J. Constr. Steel Res.*, **67**, 929-935.

Roy, K., Ting, T.C.H., Lau, H.H. and Lim, J.B.P. (2018a), "Effect of thickness on the behaviour of axially loaded back-to-back cold-formed steel built-up channel sections-Experimental and numerical investigation", *Structures*, **16**, 327-346.

Roy, K., Ting, T.C.H., Lau, H.H. and Lim, J.B.P. (2018b), "Nonlinear behaviour of back-to-back gapped built-up cold-formed steel channel sections under compression", *J. Constr. Steel Res.*, **147**, 257-276.

Roy, K., Ting, T.C.H., Lau, H.H. and Lim, J.B.P. (2018c), "Experimental investigation into the behaviour of back-to-back gapped built-up cold-formed steel channel sections under compression", *Proceedings of 'Wei-Wen Yu International Specialty Conference on Cold-Formed Steel Structures 2018'*, St. Louis, MI, USA, November.

Roy, K., Ting, T.C.H., Lau, H.H. and Lim, J.B.P. (2018d), "Nonlinear behavior of axially loaded back-to-back built-up cold-formed steel un-lipped channel sections", *Steel Compos. Struct., Int. J.*, **28**(2), 233-250. http://dx.doi.org/10.12989/scs.2018.28.2.233

Roy, K., Mohammadjani, C. and Lim, J.B.P. (2019), "Experimental and numerical investigation into the behaviour of face-to-face built-up cold-formed steel channel sections under compression", *Thin-Wall. Struct.*, **134**, 291-309.

Schafer, B.W. and Pekoz, T. (1998), "Computational modelling of cold-formed steel: characterizing Geometric imperfections and residual stress", *J. Constr. Steel Res.*, **47**, 193-210.

Shi, G., Liu, Z., Ban, H.Y., Zhang, Y., Shi, Y.J. and Wang, Y.Q. (2011), "Tests and finite element analysis on the local buckling of 420 MPa steel equal angle columns under axial compression", *Steel Compos. Struct., Int. J.*, **12**(1), 31-51. http://dx.doi.org/10.12989/scs.2011.12.1.031

Standards Australia (2018), Cold-Formed Steel Structures, AS/NZS 4600:2018, Standards Australia/ Standards New Zealand.

Stone, T.A. and LaBoube, R.A. (2005), "Behaviour of cold-formed steel built-up I-sections", *Thin-Wall. Struct.*, **43**(12), 1805-1817.

Ting, T.C.H., Roy, K., Lau, H.H. and Lim, J.B.P. (2018), "Effect of screw spacing on behavior of axially loaded back-to-back cold-formed steel built-up channel sections", *Adv. Struct. Eng.*, **21**(3), 474-487.

Vishnuvardhan, S. (2006), "Behaviour of cold-formed steel single and compound angles in compression", Ph.D. Dissertation; Anna University, Chennai, India.

Whittle, J. and Ramseyer, C. (2009), "Buckling capacities of axially loaded, cold-formed, built-up channels", *Thin-Wall. Struct.*, **47**(2), 190-201.

Yan, L., Tianhua, Z., Wenchao, L. and Hanheng, W. (2017), "Experimental investigation and a novel direct strength method for cold-formed built-up I-section columns", *Thin-Wall. Struct.*, **112**, 125-139.

Young, B. and Chen, J. (2008), "Column tests of cold-formed steel non-symmetric lipped angle sections", *J. Constr. Steel Res.*, **64**, 808-815.

Zhang, J.H. and Young, B. (2012), "Compression tests of cold-formed steel I-shaped open sections with edge and web stiffeners", *Thin-Wall. Struct.*, **52**, 1-11.

Zhou, W. and Jiang, L. (2017), "Distortional buckling of cold-formed lipped channel columns subjected to axial compression", *Steel Compos. Struct., Int. J.*, **23**(3), 331-338. http://dx.doi.org/10.12989/scs.2017.23.3.331

BU

Notations

A_g	Gross cross-sectional area (mm^2)
D	Overall lip depth
E	Modulus of elasticity (N/mm^2)
F_y	Yield strength
K	Effective length factor
L	Unbraced member length
b_o	Overall width
F_u	Ultimate tensile strength of steel (N/mm^2)
h_o	Overall depth of the channel section
r_i	Minimum radius of gyration
FE	Finite element
FEA	Finite element analysis
t	Base metal thickness
λ	Slenderness ratio
CFS	Cold-formed steel
DSM	Direct Strength Method
COV	Coefficient of variation